Society of Medical Education & Research

2026, Volume 6, Issue 1, Page No: 248-270

ISSN: 3108-4834

Archive of International Journal of Cancer and Allied Science

A Next-Generation CD19 CAR T Cell Therapy Targeting a Membrane-Proximal Epitope Overcomes Resistance in B-Cell Non-Hodgkin Lymphoma

Zsolt Kovács[1]*, Katalin Szabo[1], Gabor Nagy[2], Eszter Toth[3]

[1]Department of Lymphoma and Next-Generation CAR T Cells, Faculty of Medicine, Semmelweis University, Budapest, Hungary.

[2]Department of CD19 Epitope Targeting and Resistance, Faculty of Medicine, University of Debrecen, Debrecen, Hungary.

[3]Department of B-Cell Non-Hodgkin Lymphoma Immunotherapy, Faculty of Medicine, University of Pécs, Pécs, Hungary.

***E-mail** ✉ zsolt.kovacs@semmelweis.hu

Abstract

Although commercial anti-CD19 chimeric antigen receptor T-cell (CART19) therapies are effective in treating advanced B-cell non-Hodgkin lymphoma (NHL), the majority of patients ultimately relapse. Several factors contribute to treatment failure, such as loss of CD19 expression on tumor cells and functional exhaustion of CAR T cells. All approved CART19 products rely on the FMC63 single-chain variable fragment (scFv), which binds a membrane-distal epitope of CD19 and displays comparatively slow association (on) and dissociation (off) rates. We proposed that an alternative anti-CD19 scFv targeting a distinct membrane-proximal epitope, independent of FMC63 and possessing faster on- and off-rates, could help overcome these limitations and yield improved therapeutic results. An autologous CART19 construct incorporating 4-1BB costimulatory signaling was generated using a novel humanized chicken-derived antibody designated h1218. This antibody specifically recognizes a membrane-proximal region of CD19 and exhibits accelerated binding and release kinetics compared with FMC63. The h1218-CART19 product was assessed in laboratory and animal models designed to mimic resistance to FMC63-based therapies. A first-in-human multicenter phase I study was subsequently initiated to evaluate the clinical performance of AT101, the GMP-grade version of h1218-CART19, in individuals with relapsed or refractory (r/r) NHL. Preclinical experiments showed that h1218-CART19, unlike FMC63-CART19, efficiently eliminated lymphoma cells carrying CD19 point mutations (L174V or R163L) and those co-expressing the FMC63-CAR19 antigen, a phenomenon seen in patients who relapse following FMC63-CART19 treatment. In addition, h1218-CART19 demonstrated stronger cytotoxic activity against B-cell malignancies than FMC63-CART19 in both in vitro and in vivo settings. Mechanistic analyses indicated that the superior performance of h1218-CART19 stemmed from decreased activation-induced cell death (AICD) and greater proliferative capacity, resulting from its faster on- and off-rates. These promising findings prompted a phase I dose-escalation trial of AT101 using a 3 + 3 design across three dose levels (DL). In the 12 enrolled patients (7 DLBCL, 3 FL, 1 MCL, 1 MZL), AT101 displayed an encouraging safety profile, with grade 3 CRS observed in 8.3% (n = 1) and grade 4 ICANS in 8.3% (n = 1). Across the entire cohort, the overall response rate was 91.7%, and the complete response rate was 75.0%, rising to 100% in patients treated at DL-2 and DL-3. Greater AT101 expansion was associated with achievement of complete remission and sustained B-cell aplasia. A new CART19 therapy was developed that safely and potently targets a membrane-proximal epitope of CD19 via an scFv with rapid on- and off-rates. This product exhibited substantial clinical activity and a favorable safety profile in patients with relapsed B-cell NHL.

Keywords: CD19, CAR T cells, Resistance, CD19 mutations, Epitope masking, Lymphoma

Access this article online https://smerpub.com/

Received: 07 April 2026; **Accepted:** 20 June 2026

How to cite this article: Kovács Z, Szabo K, Nagy G, Toth E.A Next-Generation CD19 CAR T Cell Therapy Targeting a Membrane-Proximal Epitope Overcomes Resistance in B-Cell Non-Hodgkin Lymphoma. Arch Int J Cancer Allied Sci. 2026;6(1):248-70. https://doi.org/10.51847/LdyLrro6lN

Introduction

Therapies based on CD19-directed chimeric antigen receptor T (CART19) cells have yielded strong clinical results in CD19-expressing B-cell cancers. Despite this success, many patients either do not reach complete response (CR) or experience disease recurrence

following CART19 infusion, with relapse frequencies differing by malignancy subtype [1]. The binding characteristics between the CAR construct and CD19 on cancer cells are pivotal in shaping the effectiveness of CAR T cells. All currently approved commercial CART19 products in the United States—tisagenlecleucel, lisocabtagene maraleucel, axicabtagene ciloleucel, and brexucabtagene autoleucel—incorporate single-chain variable fragments (scFv) originating from the murine FMC63 anti-human CD19 antibody [2-4]. This FMC63 component recognizes an epitope positioned between exons 2 and 4 of CD19 [5]. Relapse frequently involves disappearance of the FMC63-targeted epitope on CD19, caused by point mutations or epitope masking [6-8]. Suboptimal CAR engagement with CD19 can also impair the function of CAR T cells [9-11].

Surface expression of CD19 may persist on relapsed tumors, yet the FMC63 epitope can still become unavailable for recognition by CAR19 through several processes. Such FMC63-epitope loss encompasses direct mutations in the epitope region [12] or its concealment by the CAR19 molecule itself [13]. Various CD19 point mutations have been identified in individuals with diffuse large B-cell lymphoma (DLBCL) and B-acute lymphoblastic leukemia (B-ALL) who developed resistance to CART19 treatment. A subset of these alterations specifically disrupts the FMC63-binding site, rendering FMC63-CART19 ineffective [8, 12, 14]. Earlier studies also described an additional resistance pathway in which the CAR19 gene is inadvertently introduced into leukemic B-cell blasts during manufacturing. This results in cis CAR19-CD19 interactions within the same cell, leading to epitope masking and consequent therapeutic resistance [13]. Therefore, directing CARs toward CD19 epitopes different from the FMC63 site offers a potential strategy to bypass epitope loss associated with FMC63-CART19. CAR T-cell dysfunction represents another important contributor to the limitations of FMC63-CART19. While patient-intrinsic T-cell features (such as differentiation state and exhaustion) and the suppressive tumor microenvironment play significant roles, the biophysical properties of the CAR-CD19 interaction are equally decisive for therapeutic success [15]. Notably, CARs engaging a membrane-proximal epitope of CD22 have been found to establish more effective immune synapses and achieve better tumor control in vivo than those targeting distal epitopes [16, 17]. Structural refinements to the CAR architecture, such as truncation of the scFv linker region, can also enhance target engagement by reducing intercellular distance and thereby boosting effector function [18]. In addition, the association (on) and dissociation (off) rates of CAR binding to its target influence the durability of CAR T-cell responses, with faster off-rates potentially supporting prolonged anti-tumor activity [11, 19].

In light of these relapse mechanisms after FMC63-CART19, we hypothesized that (1) a CART19 therapy aimed at a non-FMC63 epitope situated nearer the plasma membrane would circumvent epitope loss while improving T-cell performance, and (2) a CART19 product with rapid on- and off-rates would diminish activation-induced cell death (AICD) and limit T-cell impairment. To test this, we engineered a novel humanized antibody (h1218) that binds a membrane-proximal epitope of CD19, located between amino acids 51–63 (within exon 2), and exhibits fast on- and off-rates. This h1218 antibody was used to construct a CAR19 molecule containing 4-1BB and CD3ζ intracellular signaling domains. Comprehensive preclinical comparisons were performed between h1218-CART19 and standard FMC63-CART19. Following demonstration of favorable preclinical efficacy, the h1218-based product (termed AT101) advanced to a multicenter phase I first-in-human study in patients with relapsed or refractory non-Hodgkin lymphoma. Initial clinical data from this trial indicated high complete response rates and a tolerable toxicity profile.

Materials and Methods

Anti-CD19 scFv screening and lead optimization

A novel antibody specific for the extracellular domain (ECD) of human CD19, distinct from FMC63, was developed via competitive biopanning. This process utilized a recombinant human CD19 ECD fragment (M1-P278) in complex with FMC63 scFv to mask the FMC63 epitope, screened against a proprietary chicken immune library derived from chickens immunized with human CD19 (Patent US16/768412). Initial hits were identified in periplasmic extracts and verified by cell-binding ELISA on CD19-expressing Raji cells and CD19-negative K562 cells. Positive clones were converted into recombinant scFv formats with a $(G4S)_3$ linker, expressed in HEK293F cells, and purified using a C-terminal human Fc tag. The 1218 clone was advanced as

the primary candidate because of its ability to bind a distinct, non-FMC63 epitope on CD19.

To enhance binding strength, six residues within the complementarity-determining regions (CDRs) of the heavy and light chains of 1218 were subjected to random mutagenesis with NNK degenerate codons, while preserving at least 70% of the original sequence. Variants were screened for improved affinity based on EC_{50} values measured against CD19-positive Raji cells. The selected, optimized 1218 variant contained three amino acid changes in the light chain CDR3 and displayed an EC_{50} approximately 10-fold lower than that of the parental clone. Humanization was then performed via CDR grafting to lower potential immunogenicity. Appropriate human germline framework sequences were identified with IMGT/V-QUEST: IGHV3-21*04 and IGHJ5*01 for the heavy chain V and J segments, and IGLV1-51*02 and IGLJ2*01 for the light chain. The complete h1218 scFv sequence, consisting of a humanized VL, a $(G4S)_3$ linker, and a humanized VH, was chemically synthesized by GenScript (Jiangsu, China) and produced as a protein in HEK293F cells.

Epitope binning assay

Epitope binning experiments for h1218 were carried out on an 8-channel Octet QKe system (Pall ForteBio). AR2G biosensors (Cat# 18–5092) were first functionalized with 10 μg/mL FMC63 Fc, followed by loading with 10 μg/mL CD19-ECD-Ck fusion protein for 10 minutes. After baseline stabilization, 10 μg/mL of either FMC63 or h1218 was added for an additional 10-minute incubation to test for simultaneous binding. Absorbance was recorded at OD_{450} nm with a Victor X3 ELISA reader (PerkinElmer).

Generation of CD19-mutated cell lines and epitope mapping mutagenesis assay

Constructs encoding human CD19-T2A-GFP and cynomolgus CD19-T2A-GFP, together with their mutated variants (Bioneer, Daejeon, Korea), were inserted into the pLenti6.3 vector (Invitrogen; Cat# K5315-20). Chimeric CD19 molecules were assembled by overlap extension PCR and cloned into pLenti6.3 using the parental human and cynomolgus templates. Additional point mutants at critical codons were similarly generated by overlap extension PCR. Lentiviral particles were packaged in LentiX 293T cells and used to transduce target cells, which were then selected with blasticidin (Invitrogen; Cat# R210-01). Antibody recognition of individual CD19 mutant variants expressed on HEK293T cells was evaluated by flow cytometry, with mean fluorescence intensity (MFI) quantified.

Affinity measurement assay

Kinetic binding parameters for h1218 and FMC63 scFvs were assessed with the Octet platform. Purified scFvs were covalently attached to AR2G biosensor surfaces (Cat# 18–5092) using amine coupling. Serial dilutions of recombinant human CD19-ECD-Ck (M1-P278) were flowed over the sensors—ranging from 12.5 to 400 nM for h1218 and 50 to 1600 nM for FMC63. Real-time association and dissociation profiles were monitored, and kinetic constants were derived by applying a 1:1 Langmuir binding model.

Off-target scFv binding analysis: Retrogenix assay

Off-target interactions of the scFvs were examined using the Retrogenix platform. Fluorescently tagged h1218 and FMC63 scFvs were incubated with fixed HEK293 cells or slides that had been transduced with a comprehensive library of 5,484 expression vectors. Each vector co-expressed ZsGreen1 together with either a complete human transmembrane protein or a secreted protein anchored to the cell surface. Screenings were conducted in duplicate across 16 slide sets ($n = 2$ slides per set). A total of 16 primary hits, each represented by duplicate spots, were detected through quantitative fluorescence imaging of Alexa Fluor 647 and ZsGreen1 channels with ImageQuant software. These hits displayed a broad range of signal-to-background intensities, spanning from marginally detectable to robust. Confirmation experiments were performed by retesting the h1218 scFv protein on duplicate slides containing all 16 candidates. The entire process of library screening, validation, and data interpretation was executed at Retrogenix, a service unit of Charles River Laboratories.

Generation of the CAR construct and preclinical lentiviral vector production

The benchmark FMC63-CAR (CTL019) comprises the FMC63 scFv fused to 4-1BB and CD3ζ intracellular domains [20]. In parallel, the h1218-CAR was assembled with the h1218 scFv in place of FMC63 while preserving the same 4-1BB and CD3ζ components. Both CAR sequences were inserted into third-generation, replication-defective lentiviral plasmids (pTRPE or pLTG). Vector production involved seeding 8×10^6

HEK293T cells into each T175 flask in RPMI 1640 medium (Gibco; Cat# 11875–085) supplemented with 10% FBS (Gibco; Cat# 16140–071) and culturing overnight at 37 °C. Transfection was performed the next day, when cultures reached 70–80% confluence, using Lipofectamine 2000 (116 µL; Invitrogen) with packaging plasmids (up to 18 µg each) and 15 µg of CAR plasmid per flask. The transfection reagents and DNA were prepared in 4.6 mL Opti-MEM Reduced Serum medium (ThermoFisher). Culture supernatants were collected at 24 and 48 hours post-transfection, clarified through 0.45 µm filtration, and concentrated via ultracentrifugation at either 8,000 × g for 16–18 hours or 25,000 × g for 2.5 hours. Resulting lentiviral titers were quantified on HEK293T cells by flow cytometric detection with CAR-specific antibodies.

Preclinical CAR T cell production

Production of CAR T cells followed previously reported methods [21]. Primary T cells from healthy donors were isolated at the University of Pennsylvania's Human Immunology Core. Purified CD4+ and CD8+ populations were combined in equal proportions and stimulated with CD3/CD28 Dynabeads (Gibco; Cat# 40203D) at a 3:1 bead-to-cell ratio over 6 days. Transduction with lentiviral vectors was carried out on day 2 at an MOI of 1.5. After bead depletion on day 6, cell expansion and size were tracked every other day using a Multisizer 3 Coulter Counter (Beckman). Cryopreservation in 90% FBS with 10% DMSO was performed once proliferation rates stabilized and the mean cell volume approached 350 fL. Before functional evaluation, thawed CAR T cells were allowed to recover overnight at 37 °C in RPMI medium containing 10% FBS.

Cell lines and general cell culture

Human B-cell tumor lines, including Raji, Nalm6, OCI-Ly18, Toledo, and Pfeiffer, were obtained from the American Type Culture Collection (ATCC) or the Deutsche Sammlung von Mikroorganismen und Zellkulturen (DSMZ). The LentiX 293T packaging line was purchased from Takara Bio. All cell lines underwent short tandem repeat (STR) profiling for authentication at the University of Arizona and were screened for mycoplasma every two months using Lonza reagents (Cat# LT07-710). Routine propagation occurred in R10 medium, consisting of RPMI 1640 with 10% FBS, 1% GlutaMAX (Gibco; Cat# 35050–079), 1% penicillin/streptomycin (Gibco; Cat# 15140–122), and 1% HEPES (Gibco; Cat# 15630–130), maintained at 37 °C in a 5% CO_2 atmosphere.

Flow cytometry

Samples collected from in vitro cultures or animal experiments were stained with fluorescent antibodies for 15 minutes at room temperature in the dark, followed by a single wash in PBS (Gibco; Cat# 10010031) containing 2% FBS. Absolute quantification of cells (such as tumor or effector T cells) was achieved by incorporating Flow-Count Fluorospheres (Beckman Colter; Cat# 754053) according to the manufacturer's guidelines. Caspase 3/7 enzymatic activity was detected using CellEvent Caspase 3/7 Green Ready Flow (Invitrogen; Cat# C10427) according to the recommended protocol. Standard gating included an initial selection based on forward and side-scatter properties, followed by exclusion of doublets. Viability was assessed with ViaKrome 808 (Beckman Coulter; Cat# C36628). Detection of FMC63-CAR19 surface expression employed an anti-idiotype PE-conjugated reagent (Novartis). All flow cytometric data were acquired on a 6-laser CytoFLEX LS instrument (Beckman Coulter) and analyzed with FlowJo software versions 9.0 or 10 (FlowJo, LLC, BD).

Cytotoxicity assays

Target cells were modified by lentiviral delivery of a Click Beetle Green luciferase (CBGLuc)-GFP reporter and subsequently enriched by fluorescence-activated cell sorting on a FACS Melody device (BD). Short-term cytotoxicity was measured by co-incubating effector CAR T cells (or control cells) with luciferase-expressing targets at defined effector-to-target (E: T) ratios. Following incubation, D-luciferin potassium salt (Gold Biotechnology; Cat# 115144–35-9) was added to reach a final concentration of 15 mg/mL in PBS, and cultures were incubated for 10 minutes at 37 °C. Remaining viable cells were quantified by bioluminescence on a BioTek Synergy H4 reader, with data processed using Gen5 software (Agilent Technologies). Specific lysis percentages were computed by comparison to target cells incubated in the absence of effectors.

Long-term killing capacity was evaluated by seeding CAR T cells with target tumor cells at low E: T ratios (0.125:1 or 0.0625:1). Co-cultures were sampled every 48–72 hours for absolute counts of both T cells and cancer cells via flow cytometry with CountBright absolute counting beads (ThermoFisher; Cat# C36950).

Cell densities were maintained at 1×10^6 cells/mL for the duration of the assay.

Cytokine secretion assay

Target tumor cells and effector CAR T cells were co-incubated at ratios of 5:1 or 3:1 in R10 medium over 24 hours. Culture supernatants were harvested afterward and either processed promptly or frozen at -80 °C for later use. Concentrations of secreted cytokines were determined with ELISA MAX Standard Sets for human IL-2 (BioLegend; Cat# 431801) and human IFN-γ (BioLegend; Cat# 430101; BD Biosciences; Cat# 555142).

Cell avidity measurement using z-Movi

Avidity of CAR T cell binding to Nalm6 cell monolayers was quantified on a z-Movi Cell Avidity Analyzer (LUMICKS). Acoustofluidic chips were pretreated with poly-L-lysine (Sigma-Aldrich; Cat# P4707) for 3 hours to facilitate tumor cell attachment. Nalm6 cells (2×10^6 per chip) were seeded at 1×10^8 cells/mL and allowed to form a stable monolayer during a 2-hour incubation at 37 °C. Subsequently, 1×10^5 CAR T cells labeled with CellTracker Deep Red Dye (ThermoFisher; Cat# C34565) were added and permitted to interact with the monolayer for 15 minutes. An increasing acoustic force gradient was then applied to detect detachment events, which were documented and analyzed using ImageJ and R. Experiments adhered strictly to manufacturer protocols (LUMICKS), with avidity parameters calculated via the accompanying z-Movi software (v1.0).

Xenograft mouse models

Immunodeficient NOD-SCID gamma (NSG, NOD.Cg-Prkdcscid Il2rgtm1Wjl/SzJ) mice between 6 and 8 weeks of age were sourced from the Stem Cell and Xenograft Core, University of Pennsylvania, and maintained in a pathogen-free environment. Raji and Nalm6 lines were transduced to express Click Beetle Green luciferase (CBGLuc). Tumor engraftment was established by intravenous injection of 1×10^6 Nalm6 cells suspended in 0.15 mL sterile PBS via the tail vein. Tumor progression was tracked noninvasively with a Xenogen IVIS imaging system (PerkinElmer). Bioluminescence intensity (BLI) was recorded 10 minutes after luciferin administration (100 mg/kg; GoldBio; Cat# LUCK-1G). Once BLI values approached 10^7 total flux (photons per second), typically 5–7 days post-inoculation, mice were randomized to receive tail-vein infusions of specified numbers of CAR-expressing T cells or untransduced control T cells (UTD). Mice were closely observed for clinical signs of disease advancement or adverse effects, including xenogeneic graft-versus-host disease indicated by body weight reduction exceeding 10%, alopecia, diarrhea, conjunctivitis, or hind-limb paralysis. Animal husbandry and experimental procedures conformed to NIH guidelines and received approval from the University of Pennsylvania Institutional Animal Care and Use Committee (IACUC).

Confocal microscopy imaging of the immune synapse

Planar lipid bilayers were assembled on glass coverslips by fusion of small liposome vesicles, as described [22]. Liposomes were contained within a μ-Slide VI 0.4 flow chamber (Ibidi; Cat# 80606). Bilayers were blocked with 5% casein for 20 minutes, then incubated with 6.3 nM streptavidin (ThermoFisher; Cat# 434301) for 15 minutes. After rinsing with imaging buffer (HEPES-buffered saline), bilayers were functionalized with Alexa Fluor 647-conjugated biotinylated CD19 (R&D Systems; Cat# AVI9269) for 30 minutes at room temperature. Remaining streptavidin sites were quenched with 2.5 μM D-biotin. CAR T cells were added to the bilayers and stimulated for 2 hours at 37 °C. Following stimulation, cells were fixed with freshly prepared 4% paraformaldehyde for 15 minutes and permeabilized in 0.5% Triton X-100 plus 10% normal donkey serum in PBS for 30 minutes at room temperature. Immunostaining was carried out using antibodies against perforin (clone dG9; BioLegend; Cat# 308105), phospho-CD3ζ (Y83; Abcam; Cat# ab68236), and phospho-ZAP70 (Tyr319; Cell Signaling; Cat# 2701) as previously detailed [23]. Actin cytoskeleton was labeled with Alexa Fluor 405-phalloidin (ThermoFisher; Cat# A30104). Confocal images were captured on a Nikon A1R HD microscope.

General preclinical work statistical analysis

In vitro experiments were performed independently at least twice, with representative results shown. Quantitative data are expressed as individual data points or mean values ± standard error of the mean (SEM). Two-tailed unpaired Student's t-test evaluated differences between two experimental groups. For multiple group comparisons, one-way ANOVA followed by Tukey's multiple comparison test was applied unless stated otherwise. Kaplan-Meier survival curves were compared using the log-rank (Mantel-Cox) test. Significance levels

are marked as * $P < 0.05$, ** $P < 0.01$, *** $P < 0.001$, and **** $P < 0.0001$. Statistical computations and graphing were conducted in GraphPad Prism version 9.0 (San Diego, CA).

Clinical trial design

This open-label, multicenter phase I trial employed a classic 3 + 3 dose-escalation framework and was performed at two sites in South Korea. Full details regarding patient selection criteria are outlined in the main text. Following leukapheresis for collection of starting material and subsequent CAR T cell production, study participants underwent conditioning lymphodepletion with fludarabine (25 mg/m² intravenously on days -4, -3, and -2) combined with cyclophosphamide (250 mg/m² intravenously on the same days). This chemotherapy regimen matched the lymphodepletion schedule approved by the FDA for the commercial CAR T19 therapy tisagenlecleucel [24]. 30-60 minutes before CAR T cell administration, patients received premedication consisting of acetaminophen and diphenhydramine. CAR T cells were given as a single intravenous infusion across three escalating dose levels: 0.2×10^6 cells/kg (DL-1), 1.0×10^6 cells/kg (DL-2), and 5.0×10^6 cells/kg (DL-3). Because the investigational product was first-in-human, both the conditioning chemotherapy and cell infusion were performed in an inpatient hospital setting. Tumor response evaluations were scheduled at 1, 3, 6, and 12 months post-infusion or at additional time points when clinically warranted. Extended monitoring was planned for five years after treatment, on an annual basis.

The primary study endpoints focused on the safety of AT101 administration and the practicality of its manufacturing process. Secondary endpoints comprised measures of therapeutic efficacy, in vivo persistence of the CAR T cells, frequency and duration of B-cell aplasia and hypogammaglobulinemia, as well as progression-free survival (PFS) and overall survival (OS) at the one- and two-year marks.

The trial protocol was reviewed and authorized by the Ministry of Food and Drug Safety (MFDS) in Korea and by the institutional ethics committees at each participating hospital. The study is registered on ClinicalTrials.gov (NCT05338931). AbClon Inc. sponsored and oversaw the trial. Every enrolled patient granted written informed consent in line with the ethical principles of the Declaration of Helsinki. Results presented here include all individuals who received AT101 cell infusion up to the cutoff date of December 19, 2022. The final data update occurred on September 25, 2023.

Clinical-grade manufacturing of AT101 CART19 cells

Production of AT101 for clinical use complied fully with current regulations issued by the Ministry of Food and Drug Safety (MFDS), South Korea's regulatory body. Manufacturing was carried out in a closed, automated system using the CliniMACS Prodigy platform (Miltenyi Biotec). Apheresis material was processed with the TS520 tubing set, enabling magnetic selection and enrichment of CD4+ and CD8+ T cell subsets. An initial inoculum of 5×10^7 CD3+ T cells was introduced into the device, activated via anti-CD3/CD28 TransAct beads (Miltenyi), and cultured in the presence of supplemental IL-2 (MACS GMP Recombinant Human IL-2, Miltenyi). Transduction with clinical-grade h1218 lentiviral particles (Lentigen) occurred on day 1 at a multiplicity of infection of 1, after which cells were expanded to a target maximum of 4×10^9 cells. In keeping with MFDS requirements, release criteria included culture-based assays for replication-competent lentivirus (RCL), adventitious viruses, and product sterility.

Toxicity and response assessment

Grading of cytokine release syndrome (CRS) and immune effector cell-associated neurotoxicity syndrome (ICANS) adhered to the consensus criteria established by the American Society for Transplantation and Cellular Therapy [25]. Additional adverse events were scored using the Common Terminology Criteria for Adverse Events (CTCAE) version 5.0. Radiologic responses in lymphoma patients were interpreted from PET-CT, CT, or MRI scans according to the Lugano classification system [26].

Statistical analysis for the clinical trial

Continuous data are presented as median values with ranges (unless otherwise noted), and categorical data are summarized as percentages. Progression-free survival was computed as the interval from AT101 infusion to the first occurrence of disease progression, death from any cause, or last contact. Overall survival was defined as the time from infusion to death or last follow-up. All statistical evaluations and graphical outputs were generated using GraphPad Prism version 9.5.0 (730). Because the principal goal of this phase I investigation was to identify the maximum tolerated dose (MTD) and

the recommended phase II dose (RP2D) through evaluation of safety and tolerability, formal hypothesis testing was not undertaken.

Results and Discussion

Discovery of h1218: A novel humanized chicken-derived scFv targeting a membrane-proximal epitope on human CD19

In this study, we aimed to generate an antibody directed against a CD19 epitope that differs from the epitope bound by the FMC63 antibody employed in all existing FDA-approved CART19 therapies **(Figure 1a)**. For this purpose, a proprietary chicken immune single-chain variable fragment (scFv) library was screened using the extracellular domain of human CD19 (M1-K291). Because the evolutionary divergence between chickens and humans is greater than that between mice and humans, chicken-derived libraries enable the isolation of antibodies that recognize epitopes typically inaccessible to conventional murine antibodies. From an initial panel of six candidate clones, we selected clone 1218 because it failed to compete with FMC63 for binding to CD19 (M1-P278). Subsequent epitope binning analysis conducted on the Octet platform confirmed that h1218 and FMC63 can bind concurrently to CD19 **(Figure 1b)**, thereby establishing that they engage non-overlapping epitopes. The parental chicken 1218 scFv was humanized via CDR grafting onto human germline gene frameworks, supplemented by appropriate back-mutations, to produce the humanized variant designated h1218.

Epitope mapping was performed using domain swapping and site-directed mutagenesis. The extracellular portion of CD19 was segmented into three structural domains. Each human (H) domain was replaced individually with its cynomolgus monkey (C) counterpart, yielding the chimeras H–H-H-(cell), C-H–H-(cell), H-C-H-(cell), and H–H-C-(cell). Binding assays revealed that h1218 recognized the H–H-C chimera but failed to bind the C-H–H variant. This pattern indicated that h1218 interacts with an epitope located in the membrane-proximal domain, specifically within residues 51–63, in contrast to the binding site of FMC63 **(Figure 1c)**. Alanine-scanning mutagenesis further identified L58, K59, and K63 as critical contact residues for h1218 scFv binding. By comparison, residue H218/KSS [27] served as a key determinant for FMC63 recognition **(Figure 1d)**. Functional validation by ELISA showed a pronounced reduction in interferon-gamma secretion by h1218-CART19 cells when L58, K59, or K63 was mutated. Substitutions at T51, S53, and E55 produced more modest decreases in cytokine production **(Figure 1e)**. Surface plasmon resonance analysis demonstrated that h1218 and FMC63 scFvs possess similar overall affinities for CD19-ECD-Ck (mean KD of $1.85 \times 10{-}7$ M and $1.49 \times 10{-}7$ M, respectively). However, their kinetic profiles differed markedly **(Figure 1f)**, with h1218 exhibiting a substantially higher on-rate (mean Kon: FMC63 = 8.94×103 $M^{-1}s^{-1}$ versus h1218 = 8.68×104 $M^{-1}s^{-1}$) and a faster off-rate (mean Koff: FMC63 = 1.31×10^{-3} s^{-1} versus h1218 = 1.60×10^{-4} s^{-1}).

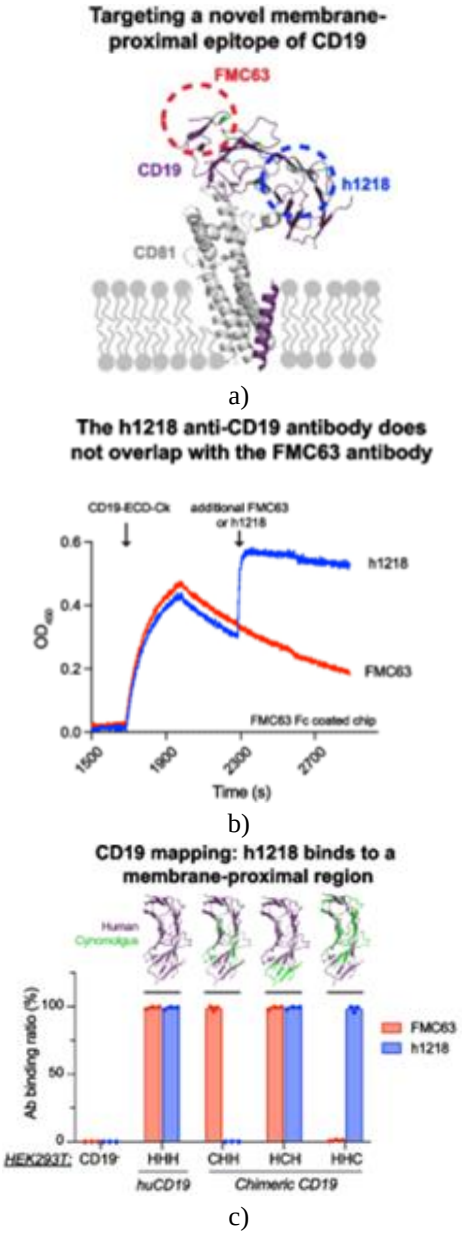

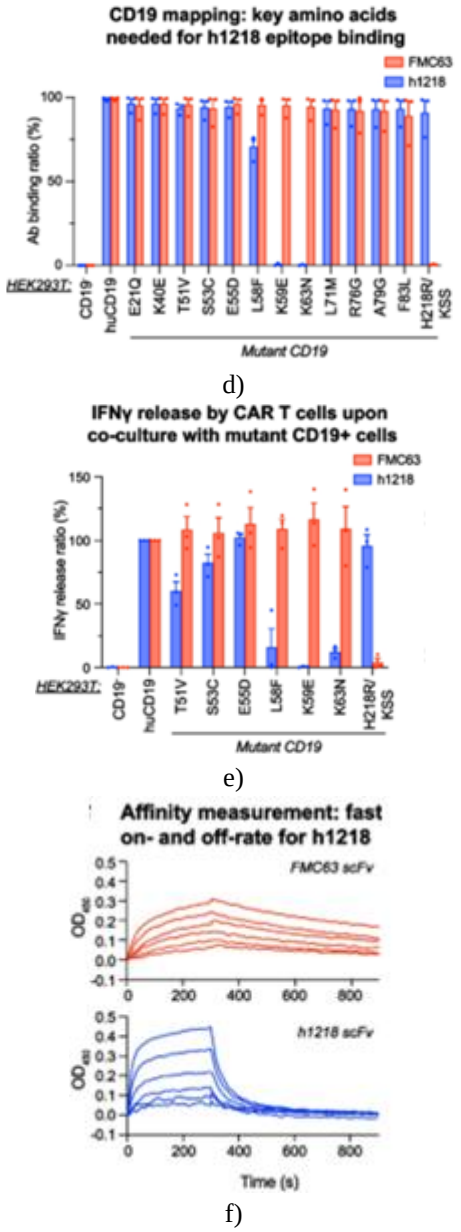

Figure 1. The h1218 antibody exhibits high specificity for CD19. It binds a membrane-proximal epitope distinct from the FMC63 binding site

(a) Diagram illustrating the respective binding locations of FMC63 and h1218 on the CD19 molecule, (b) Evaluation of h1218 binding capacity to CD19 pre-complexed with FMC63. Sensor chips coated with FMC63 Fc and CD19-ECD-Ck were loaded between 1700 and 2300 s, followed by addition of either FMC63 or h1218 at 2300 s to monitor additional association, (c) Flow cytometric assessment of h1218 binding to parental HEK293T cells (CD19-negative), HEK293T cells expressing full-length human CD19 (huCD19, HHH), and HEK293T cells expressing chimeric CD19 constructs harboring cynomolgus substitutions in individual domains (CHH, HCH, HHC), (d) Alanine-scanning mutagenesis to determine amino acid residues essential for the h1218 CD19 epitope, (e) Measurement of IFNγ release by h1218-CART19 cells co-cultured with HEK293T cells expressing either wild-type or mutant forms of CD19 to confirm additional functionally relevant residues, (f) Kinetic binding analysis of FMC63 and h1218 scFvs to recombinant human CD19-ECD-Ck (M1-P278). Curves represent measurements performed at varying scFv concentrations. All experiments were independently repeated at least twice.

To rigorously assess specificity, the h1218 scFv was screened for reactivity against a comprehensive panel of 5,484 human plasma membrane proteins and cell surface-tethered secreted proteins expressed in HEK293 cells (Retrogenix platform). Intense binding was detected solely to CD19, with only weak interactions observed for three unrelated proteins: TMEM108, SUSD5, and GUCA2A. Follow-up experiments using flow cytometry and ELISA confirmed that overexpression of TMEM108, SUSD5, or GUCA2A in HEK293T cells did not trigger activation of h1218-CART19 cells. These data conclusively excluded any meaningful off-target recognition of TMEM108, SUSD5, or GUCA2A.

h1218-CART19 effectively circumvents resistance driven by loss of the FMC63 epitope in preclinical models

After engineering a novel scFv specific for a membrane-proximal region of CD19, we designed a complete second-generation CAR construct. Lentiviral vectors (pTRPE or pLTG) served as the delivery platform, incorporating a CD8α-derived hinge and transmembrane region as well as 4-1BB costimulatory and CD3ζ signaling elements. Primary human T cells were transduced with the resulting lentiviruses and expanded ex vivo using previously reported methods [20, 21]. The new therapeutic candidate, h1218-CART19, was subsequently evaluated in models resistant to FMC63-based therapy. Two clinically observed mutations in exon 3 of CD19 (R163L and L174V) have been shown to abolish the FMC63 epitope and render cells insensitive to FMC63-CART19 [8, 14]. To recreate this resistance phenotype, wild-type CD19 was deleted from the Nalm6 B-ALL cell line via CRISPR-Cas9 gene editing. These CD19-knockout cells were then reconstituted with lentiviral vectors expressing either the

R163L or L174V mutant protein (Nalm6-CD19R163L and Nalm6-CD19L174V, respectively) **(Figure 2a)**. Surface display of the mutant CD19 variants was validated by flow cytometry **(Figure 2b)**.

Functional testing demonstrated that h1218-CART19, unlike FMC63-CART19, mediated potent killing of both mutant cell lines in vitro. In contrast, untransduced control T cells showed no activity **(Figure 2c)**. Correspondingly, co-culture with either Nalm6-CD19R163L or Nalm6-CD19L174V triggered robust secretion of IL-2 and TNF by h1218-CART19 cells, whereas FMC63-CART19 cells produced negligible cytokine levels ($P < 0.0001$ for both) **(Figure 2d)**. In vivo efficacy was assessed using the more prevalent L174V mutant. NSG mice received intravenous inoculation of 1×106 luciferase-labeled Nalm6-CD19L174V cells on day -5, followed by randomization on day 0 to treatment with 0.75×106 untransduced T cells, FMC63-CART19, or h1218-CART19 **(Figure 2e)**. Mice treated with h1218-CART19 exhibited substantially better tumor burden control and markedly extended survival relative to the FMC63-CART19 group (median survival: 9 days for FMC63-CART19 versus not reached for h1218-CART19, $P = 0.0027$) **(Figures 2e and 2f)**. In addition, h1218-CART19 cells demonstrated superior expansion in peripheral blood (mean count: 68 cells/100 µL for FMC63-CART19 versus 300 cells/100 µL for h1218-CART19, $P = 0.0096$) **(Figure 2g)**. These findings highlight the capacity of h1218-CART19 to successfully address resistance mechanisms associated with FMC63 epitope loss.

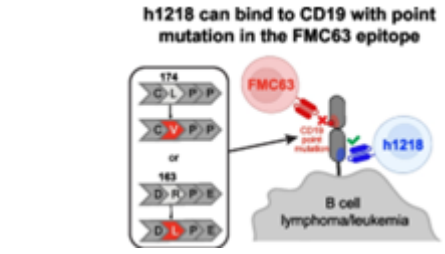

a)

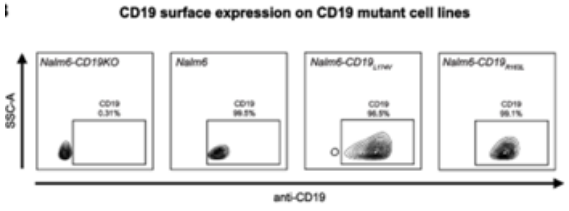

b)

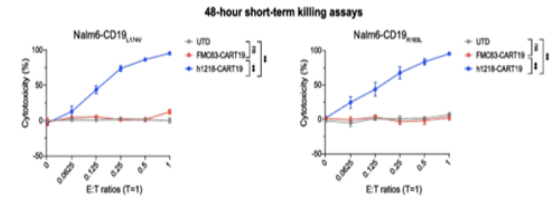

c)

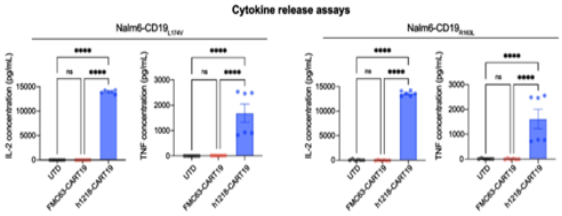

d)

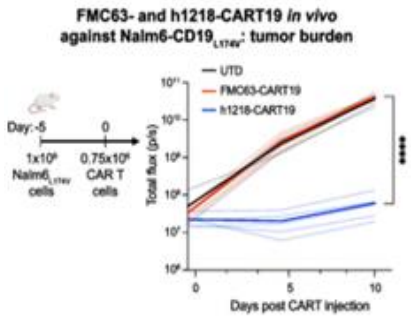

e)

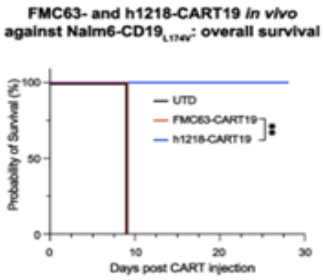

f)

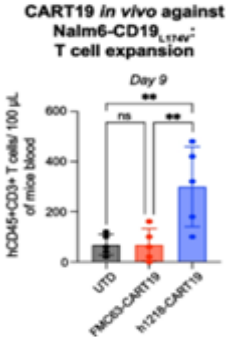

g)

Figure 2. h1218-CART19 specifically recognizes and eliminates B-cell leukemia cells bearing clinically relevant FMC63-resistant mutations in CD19

(a) Illustration of engineered leukemia cells expressing point mutations (CD19R163L or CD19L174V) within the membrane-distal portion of CD19, replicating alterations detected in patients following FMC63-CART19 relapse, (b) Representative flow cytometry histograms showing CD19 surface levels on Nalm6-CD19KO, wild-type Nalm6, Nalm6-CD19L174V (left panel), and Nalm6-CD19R163L (right panel), (c) Dose-dependent cytotoxicity of different CART19 products toward Nalm6-CD19L174V and Nalm6-CD19R163L targets across a range of effector-to-target ratios (n = 3 independent donors, luciferase assay), (d) ELISA quantification of IL-2 and TNF release after 24-hour co-incubation of effector and target cells at an E:T ratio of 5:1 (n = 2 donors). Measurements falling below the standard curve are reported as zero. (e) (Left) Overview of the NSG xenograft experimental setup: 1 × 106 luciferase-positive Nalm6-CD19L174V cells were administered on day -5, followed five days later by intravenous delivery of 0.75 × 106 UTD, FMC63-CART19, or h1218-CART19 cells. (Right) Serial bioluminescence measurements of tumor progression in mice receiving UTD (n = 5), FMC63-CART19 (n = 5), or h1218-CART19 (n = 5). Bold lines denote group medians, (f) Kaplan-Meier analysis depicting overall survival across treatment cohorts (P = 0.0027), and (g) Enumeration of circulating human CD45+CD3+ T cells per 100 µL of blood collected on day 9. All quantitative graphs and killing curves represent mean ± SEM. Survival curves were evaluated using the log-rank (Mantel-Cox) test; one-way ANOVA with Tukey's multiple comparison correction was applied for other analyses; **** P < 0.0001, *** P < 0.001, ** P < 0.01, * P < 0.05. Experiments were performed independently at least twice.

An infrequent yet important cause of FMC63 epitope loss arises from unintended transduction of leukemic B-cell blasts with the FMC63-CAR19 lentiviral construct during manufacturing. This event leads to epitope masking via intracellular (cis) binding between the CAR and endogenous CD19. Earlier studies established that such CAR19-expressing B-ALL blasts resist FMC63-CART19 killing even when CD19 remains detectable on the cell surface [12]. Given that h1218 engages a separate epitope, we anticipated that h1218-CART19 would retain recognition of these masked targets. To test this hypothesis, we generated Nalm6 cells co-expressing native CD19 and the FMC63-CAR19 construct (Nalm6-FMC63) **(Figures 3a and 3b)**. These engineered cells had been previously confirmed to be refractory to FMC63-CART19 [12].

In vitro assays demonstrated that h1218-CART19 induced potent short-term and sustained cytotoxicity along with substantial IL-2 release when cultured with Nalm6-FMC63 cells. In contrast, FMC63-CART19 exhibited minimal functional activity against the same targets **(Figures 3c-3e)**. These promising results were subsequently evaluated in vivo. NSG mice were intravenously injected with 1 × 106 Nalm6-FMC63 cells on day -5 and then assigned on day 0 to treatment groups receiving 0.75 × 106 untransduced T cells, FMC63-CART19, or h1218-CART19 **(Figure 3f)**. Animals treated with h1218-CART19 displayed significantly superior tumor suppression and extended survival compared with those receiving FMC63-CART19 (median overall survival: 7 days versus not reached, P = 0.0016) **(Figures 3f and 3g)**. Overall, the findings indicate that h1218-CART19, by targeting a membrane-proximal CD19 epitope, can effectively target and control leukemic cells that have developed resistance through either mutational epitope loss or FMC63-CAR-mediated masking.

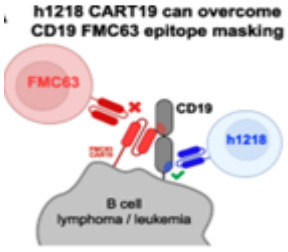

a)

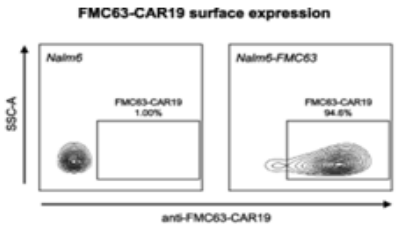

b)

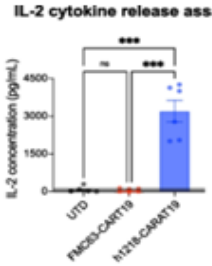

c)

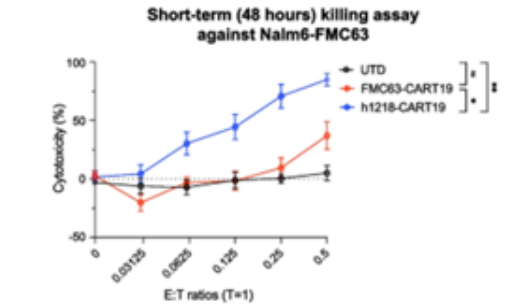

d)

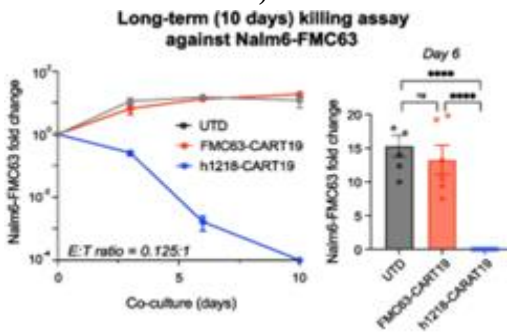

e)

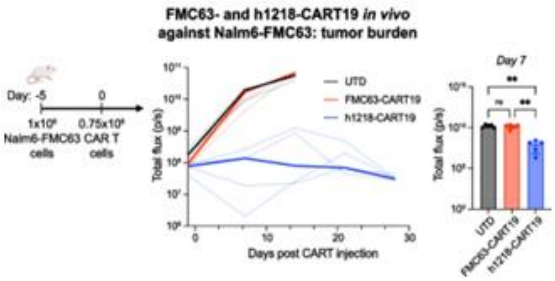

f)

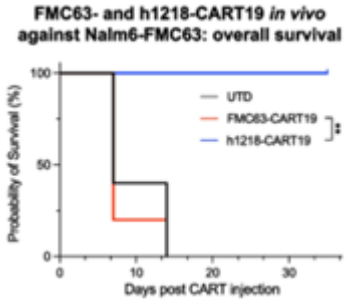

g)

Figure 3. h1218-CART19 detects and destroys relapsed Nalm6 cells positive for FMC63-CAR19

(a) Diagram depicting leukemic B cells that have undergone accidental transduction with the FMC63-CAR19 vector, resulting in epitope masking and consequent resistance to standard FMC63-CART19 therapy, (b) Flow cytometry analysis of FMC63 expression on the surface of modified Nalm6 cells, (c) ELISA-based determination of IL-2 levels released 24 hours following co-culture of CART19 effectors with Nalm6-FMC63 targets at an E: T ratio of 5:1 (n = 2 donors). Readings below the standard curve threshold are recorded as zero, (d) Evaluation of 48-hour cytotoxicity mediated by CART19 products against Nalm6-FMC63 cells at different effector-to-target ratios (n = 2 donors) using flow cytometry, (e) Monitoring of tumor cell expansion in the presence of CART19 cells over a 10-day culture period (n = 3 donors) by flow cytometry. (Left) Temporal fold-change in Nalm6-FMC63 cell numbers relative to baseline (day 0). (Right) Specific fold-change observed on day 6, (f) (Left) Design of the NSG xenograft experiment: 1 × 106 luciferase-positive Nalm6-FMC63 cells were implanted five days before intravenous delivery of 0.75 × 106 UTD or CART19 cells. (Right) Serial bioluminescence tracking of tumor progression in mice bearing Nalm6-FMC63 tumors following treatment with UTD (n = 5), FMC63-CART19 (n = 5), or h1218-CART19 (n = 5). Bold lines correspond to median values per group, and (g) Survival curves for mice engrafted with Nalm6-FMC63 cells ($p = 0.0016$). All quantitative data are shown as mean ± SEM. One-way ANOVA with Tukey's post-test was used for group comparisons, and survival was analyzed by the log-rank (Mantel-Cox) method; **** $P < 0.0001$, *** $P < 0.001$, ** $P < 0.01$, * $P < 0.05$. All experiments were performed independently at least twice.

Superior therapeutic performance of h1218-CART19 relative to FMC63-CART19 in preclinical human B-cell malignancy models

Consistent with the distinct kinetic profile of the h1218 scFv, which features accelerated on- and off-rates compared with FMC63, we reasoned that a CAR based on h1218 might yield better therapeutic results. This advantage was expected to stem from decreased susceptibility to activation-induced cell death (AICD) during antigen encounter **(Figure 4a)**. The functional superiority of h1218-CART19 over standard FMC63-CART19 was therefore investigated in a series of relevant in vitro and in vivo models of B-cell lymphoma and acute lymphoblastic leukemia. When evaluated in standard short-term (48-hour) killing assays, both CAR T-cell products displayed comparable lytic capacity toward Nalm6 and additional hematologic cancer cell lines **(Figure 4b)**. Similarly, no substantial differences in IFNγ secretion were detected between the two constructs

upon brief exposure to various CD19-positive targets, including Raji (Burkitt lymphoma), Pfeiffer (DLBCL), Toledo (DLBCL), and Nalm6 (B-ALL) cells **(Figure 4c)**. In vivo, h1218-CART19 showed clear dose responsiveness against Raji xenografts, and at a high cell dose of 1.5 × 106 CAR T cells, both products achieved equivalent tumor clearance in mice bearing Raji or Nalm6 tumors **(Figure 4d)**.

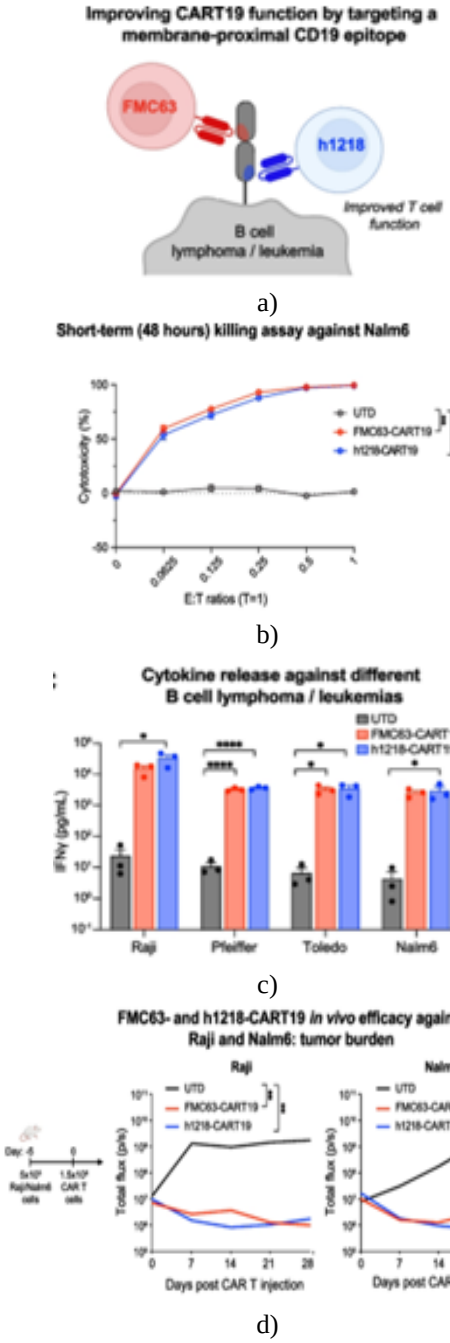

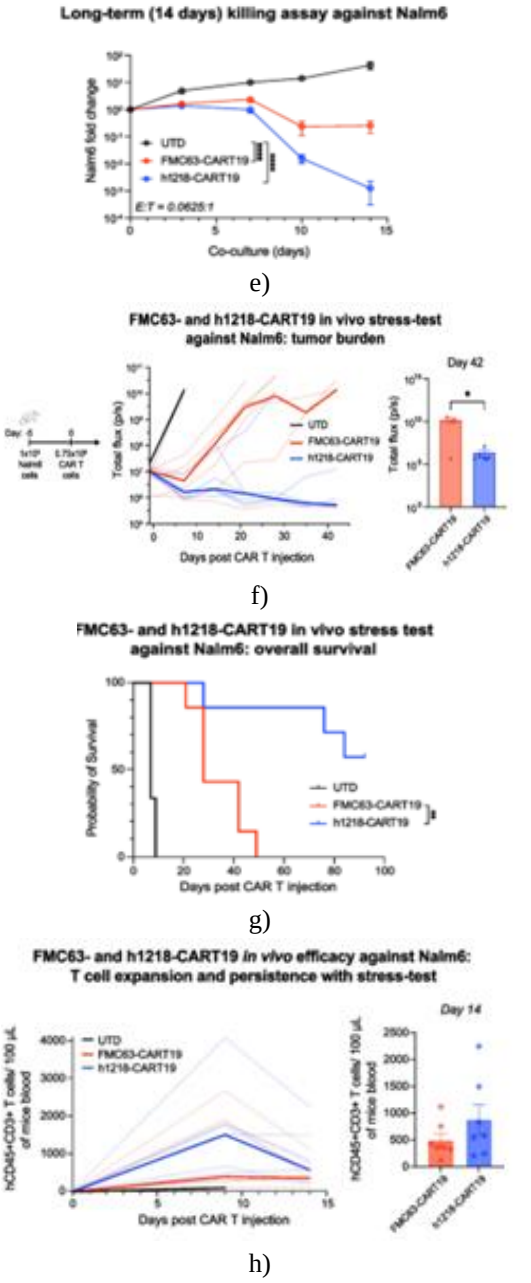

Figure 4. h1218-CART19 exhibits greater anti-tumor potency than FMC63-CART19

(a) Diagram highlighting the membrane-proximal binding mode of h1218-CART19 on malignant B cells in contrast to conventional FMC63-CART19, (b) Flow cytometric measurement of Nalm6 cell lysis by UTD, h1218-CART19, or FMC63-CART19 effectors at increasing effector-to-target ratios (n = 3 donors), (c) ELISA quantification of IFNγ levels released after stimulation with CD19-expressing lines (Raji, Pfeiffer, Toledo, Nalm6) at an E: T ratio of 3:1 (n = 2 donors), (d)

(Left) Experimental timeline for the high-dose in vivo study: 1.5 × 106 UTD or CART19 cells were infused seven days following intravenous administration of luciferase-labeled Raji or Nalm6 cells. Tumor burden kinetics are presented for Raji (middle) and Nalm6 (right) models. (e) Long-term control of Nalm6 proliferation over 14 days at low E:T ratios in the presence of UTD, FMC63-CART19, or h1218-CART19 (n = 2 donors) determined by flow cytometry. (f) (Left) Outline of the low-dose stress-test xenograft protocol: 0.75 × 106 UTD or CAR T cells were given five days after Nalm6-luciferase engraftment. (Middle) Serial bioluminescence imaging of tumor load in mice treated with UTD (n = 3), FMC63-CART19 (n = 7), or h1218-CART19 (n = 7). Bold lines denote group medians. (Right) Tumor burden assessment on day 42 post-treatment, (g) Survival analysis of mice with Nalm6 xenografts, and (h) (Left) Time course of CAR T-cell expansion in peripheral blood. Bold lines show median values. (Right) Absolute CAR T-cell counts in blood on day 14 post-infusion measured by flow cytometry. All graphs and curves represent mean ± SEM. Statistical tests included Student's t-test for pairwise comparisons, one-way ANOVA with Tukey's correction for multi-group analyses, and log-rank (Mantel-Cox) for survival; **** $P < 0.0001$, *** $P < 0.001$, ** $P < 0.01$, * $P < 0.05$. All experiments were conducted independently at least twice.

However, under more stringent "stress-test" conditions using lower, suboptimal CAR T-cell doses (0.75 × 106 cells), clear advantages emerged for h1218-CART19. In extended low-ratio in vitro co-cultures (E: T 0.0625:1), h1218-CART19 achieved markedly better sustained suppression of Nalm6 cell outgrowth than FMC63-CART19 **(Figure 4e)**. Parallel in vivo experiments employing the same reduced cell dose in NSG mice confirmed significantly enhanced tumor control by h1218-CART19 ($P = 0.042$) **(Figure 4f)**. This improved efficacy correlated with prolonged animal survival (median survival not reached for h1218-CART19 versus 28 days for FMC63-CART19, $P = 0.0017$) **(Figure 4g)**. Furthermore, h1218-CART19 demonstrated superior expansion and persistence in the circulation compared with FMC63-CART19 **(Figure 4h)**. In summary, these preclinical data establish that h1218-CART19 confers stronger antileukemic and antilymphoma activity than FMC63-CART19, linked to enhanced CAR T-cell proliferation and durability in vivo.

Faster association and dissociation kinetics of h1218-CART19 cells correlate with reduced activation-induced cell death relative to FMC63-CART19

To elucidate the functional attributes and mechanistic basis for the superior anti-tumor performance of h1218-CART19 in comparison with FMC63-CART19, cellular interactions between CART19 effectors and tumor targets were investigated. In accordance with the premise that the accelerated on- and off-rates of the h1218 scFv underpin enhanced CAR T-cell functionality, cellular avidity was quantified for FMC63-CART19 and h1218-CART19 using the z-Movi platform (LUMICKS). Consistent with earlier scFv affinity measurements, h1218-CART19 cells displayed substantially lower cellular avidity than FMC63-CART19 cells (mean avidity, FMC63 = 55.57% versus h1218 = 39.23%, $P < 0.0001$) **(Figure 5a)**.

The immune synapse properties of the respective CAR T cells were subsequently examined using established protocols [28]. Synapse stability was evaluated through F-actin quantification, and physical synapse assembly was assessed via CD19 clustering. In keeping with the diminished avidity observed for h1218-CART19 versus FMC63-CART19, both F-actin accumulation at the synapse and CD19 protein recruitment were attenuated in h1218-CART19 cells. Early CAR signaling events were further analyzed by assessing the polarization of perforin and phosphorylated CD3ζ (pCD3ζ) toward the immunological synapse. Consistent with these patterns, h1218-CART19 cells exhibited reduced perforin and pCD3ζ localization at the synapse after 2-h stimulation compared with FMC63-CART19 cells **(Figures 5b and 5c)**. Such findings correspond with the more rapid off-rate of h1218.

Considering the improved anti-tumor potency and in vivo expansion of h1218-CART19 observed in prior studies, it was postulated that h1218-CART19 is more effective than FMC63-CART19 by attenuating initial CAR T-cell activation and activation-induced cell death (AICD), thereby enhancing CAR T-cell survival upon tumor contact. This premise was tested by quantifying AICD following target engagement. Importantly, h1218-CART19 demonstrated lower baseline caspase 3/7 cleavage and markedly decreased AICD, as evidenced by caspase 3/7 cleavage post-stimulation, compared with FMC63-CART19 **(Figure 5d)**. These data indicate heightened AICD in FMC63-CART19 cells, potentially accounting for diminished long-term T-cell persistence.

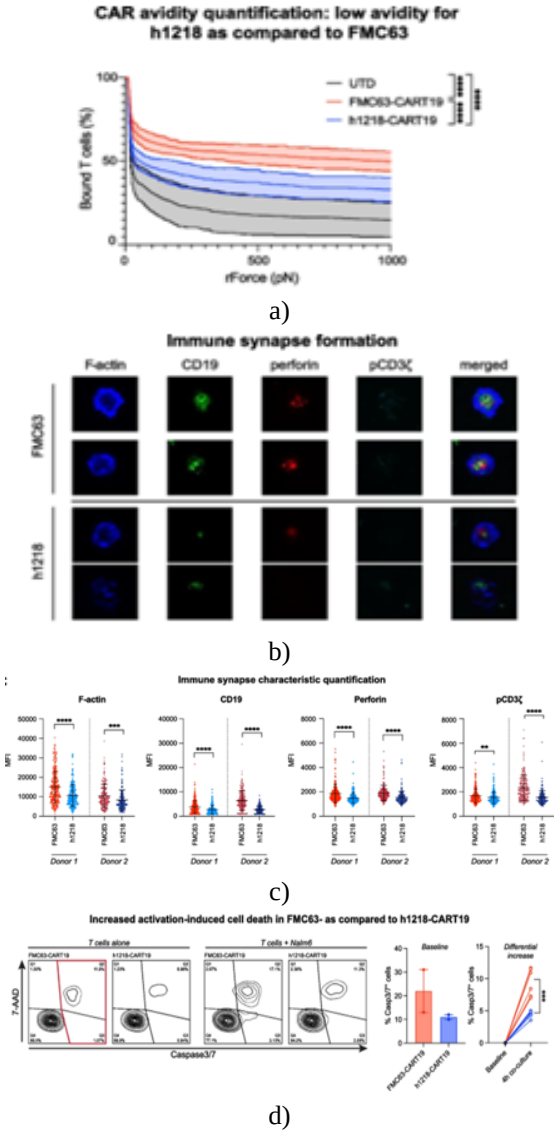

Figure 5. h1218-CART19 displays reduced cellular avidity and diminished activation-induced cell death in comparison with FMC63-CART19.

(a) Measurement of binding avidity for UTD, FMC63-CART19, and h1218-CART19 cells to Nalm6 after 15-min co-incubation (n = 2 donors) via Lumicks analysis, (b) Representative confocal microscopy images depicting F-actin, CD19, perforin, and phosphorylated-CD3ζ (pCD3ζ) (CAR) in FMC63-CART19 or h1218-CART19 cells following engagement with biotinylated CD19 protein, (c) Quantitative analysis of F-actin, perforin polarization, and pCD3ζ in FMC63-CART19 or h1218-CART19 cells interacting with biotinylated CD19 protein (n = 2 donors). A total of 200 events were evaluated for each condition, and (d) (Left) Representative flow cytometry plots showing Caspase3/7+ populations in FMC63-CART19 and h1218-CART19 cells, with or without 4-h Nalm6 stimulation. The Caspase3/7+ CART19 population is outlined in red. (Middle) Baseline Caspase3/7+ levels in FMC63- or h1218-CART19 cells at 0 h. (Right) Change in the Caspase3/7+ population following 4-h stimulation. All data are shown as mean ± SEM. Student's t-test was employed for two-group comparisons; one-way ANOVA with Tukey's post-hoc correction was applied for multiple comparisons; **** $P < 0.0001$, *** $P < 0.001$, ** $P < 0.01$, and * $P < 0.05$. All bar graphs present mean ± SEM values. Experiments were performed at least twice with similar results.

First-in-human study of h1218-CART19 for patients with relapsed or refractory non-hodgkin lymphoma: trial design and participant profile

Following encouraging preclinical findings with h1218-CART19, the candidate was advanced to a clinical-grade, good manufacturing practice (GMP) product, AT101 (AbClon Inc.). A phase I/II multicenter first-in-human trial was launched to assess the safety and establish the recommended phase II dose (RP2D) of AT101 in individuals with B-cell non-Hodgkin lymphoma (NCT05338931). The protocol followed a classic 3 + 3 dose-escalation framework (see "Methods" section). This report summarizes the preliminary outcomes from the Phase I component of the study.

Main eligibility requirements included histologically confirmed B-cell non-Hodgkin lymphoma that had relapsed or proven refractory to at least one standard regimen, ECOG performance status of 0–1, and adequate function of key organ systems including hematologic, renal, hepatic, pulmonary, cardiac, and bone marrow reserves. Participants with histories of cellular therapies, autologous stem cell transplantation (ASCT), or CD3/CD20 bispecific antibodies were permitted to enroll. After initial screening, eligible patients provided written informed consent. Autologous T lymphocytes were harvested by standard leukapheresis and engineered into the AT101 product using automated, closed-system manufacturing. Dose level allocation occurred following apheresis completion. Before infusion, patients underwent lymphodepletion with intravenous fludarabine (25 mg/m²) plus cyclophosphamide (250 mg/m²) on days -4, -3, and -2. AT101 was delivered as a single intravenous infusion at one of three dose levels (DL): DL-1: 0.2×10^6 cells/kg, DL-2: 1.0×10^6 cells/kg, or DL-3: 5.0×10^6 cells/kg.

Bridging therapy may be administered at the investigator's discretion throughout the manufacturing interval and up to 2 weeks before the AT101 infusion.

According to the CONSORT flow diagram, 14 patients were registered and enrolled, of whom 12 (85.7%) ultimately received the infusion. Infusion was not performed in two cases due to manufacturing challenges: insufficient CAR T-cell expansion in one patient (fold expansion of 0.70 on day 6) and bacterial contamination of the apheresis material in the other, attributed to asymptomatic bacteremia likely due to intestinal bacterial translocation. Manufactured AT101 products achieved a median of 5.6 population doublings (range 5.2–6.0). The final product displayed a median CD4/CD8 ratio of 0.8 (0.1–1.7), with 92% (86–95%) of cells being $CD45^+CD3^+$ T cells. CAR^+ cells constituted a median of 46% (25–57%) of the AT101 population. The median interval from vein-to-vein was 56 (48–97) days, largely due to the time-intensive culture-dependent release and quality control assays outlined in the Methods.

Demographic and disease features of the 12 participants who received infusion are outlined in **Table 1**. Median age was 62.5 years (range 39–84), and 58.3% (7/12) were female. Participants had undergone a median of 3 prior treatment lines (range 2–8). Lymphoma histologies included diffuse large B-cell lymphoma (DLBCL, n = 7/12, 58.3%), follicular lymphoma (FL, n = 3/12, 25.0%), mantle cell lymphoma (MCL, n = 1/12, 8.3%), and marginal zone lymphoma (MZL, n = 1/12, 8.3%). Three patients presented with ECOG status 0 and nine with status 1. Previous autologous stem cell transplantation had been performed in five patients (41.7%), one patient (8.3%) had received non-gene-edited NK-cell therapy, and three (25%) had been exposed to CD20/CD3 bispecific antibodies. Refractory disease was documented in two patients (16.7%). Median sum of the product of diameters (SPD) on CT scan measured 1,041 mm^2 (range 190–11,836). Two patients (patient 9 and patient 12) received bridging therapy with CHOP or ESHAP regimens; patient 9 showed no response, while patient 12 achieved a partial response. Elevated LDH levels were observed in 5 patients (41.7%), and bulky disease (> 7 cm) was noted in 1 patient. Collectively, the enrolled cohort consisted of heavily pretreated patients, many of whom had received prior novel T-cell immunotherapies, although none had received prior CART19 treatment.

Table 1. Baseline patient characteristics.

Baseline characteristic	Value, n (%)
Age, years	
< 60	5 (41.7)
≥ 60	7 (58.3)
Median age (range)	62.5 (39–84)
Disease subtype, n (%)	
Diffuse large B-cell lymphoma (DLBCL)	7 (58.3)
Follicular lymphoma (FL)	3 (25.0)
Mantle cell lymphoma (MCL)	1 (8.3)
Marginal zone lymphoma (MZL)	1 (8.3)
Previous autologous stem cell transplantation, n (%)	5 (41.7)
Number of previous treatment lines, n (%)	
≤ 2 prior therapies	5 (41.7)
≥ 3 prior therapies	7 (58.3)
Median number of prior therapies (range)	3 (2–8)
Chemotherapy-refractory disease, n (%)	2 (16.7)
Bridging therapy administered before CAR T-cell infusion[a], n (%)	2 (16.7)

Abbreviations: DLBCL = diffuse large B-cell lymphoma, FL = follicular lymphoma, MCL = mantle cell lymphoma, MZL = marginal zone lymphoma, ASCT = autologous stem cell transplantation

Note: Bridging therapy refers to any treatment administered between leukapheresis and the start of lymphodepleting chemotherapy.

Safety profile of h1218-CART19 among individuals with relapsed or refractory B-cell non-hodgkin lymphoma

Infusion-associated acute toxicities were absent in all cases. Overall, 58.3% of treated patients developed one or more adverse events of grade ≥ 3 severity **(Table 2)**. Neutropenia emerged as the predominant serious toxicity, impacting seven individuals and largely attributable to the lymphodepletion conditioning. Six of

the 12 patients presented with B-cell counts below 50 cells/μL before conditioning. Universal B-cell aplasia developed in all participants following lymphodepletion and subsequent AT101 administration. Patient 8, who experienced disease progression at the three-month mark, showed B-cell reconstitution concurrent with tumor relapse. Grade 3 anemia occurred in 4 patients (33.3%), and grade ≥ 3 thrombocytopenia was observed in 2 patients (16.7%). Both hemoglobin and platelet levels declined in the immediate post-lymphodepletion period but recovered rapidly among those who achieved a disease response. Serum ferritin reached maximal concentrations in the initial two weeks after AT101 delivery. One individual (patient 12) developed grade 3 sepsis on day 19 that responded promptly to antibiotics; nevertheless, 27 days following the initial episode, candidemia-triggered septic shock ensued, culminating in fatal multi-organ dysfunction **(Table 2)**.

Cytokine-release syndrome (CRS) affected 33.3% of the cohort (n = 4), reaching grade 3 severity in a single patient (8.3%). CRS was not observed at DL-1. At higher dose levels (DL-2/3), three patients manifested grade 1 CRS and one patient at DL-3 developed grade 3 CRS. CRS typically began at a median of 6.5 days (range 2–11) post-infusion and resolved rapidly, usually within one day. Steroid therapy was unnecessary for CRS management in any case. Immune effector cell-associated neurotoxicity syndrome (ICANS) arose in 25% of patients (n = 3). A single grade 4 ICANS event (8.3%) occurred at DL-1 and represented the trial's only dose-limiting toxicity (DLT). This patient developed encephalopathy on day 12, requiring temporary intubation, but achieved complete neurological recovery following six days of intravenous dexamethasone combined with intrathecal hydrocortisone. Following this DLT, the DL-1 cohort was expanded by three additional patients, none of whom exhibited ICANS. Grade 1–2 neurotoxicity was documented in one DL-2 patient (tremors) and one DL-3 patient (delirium). ICANS onset occurred at a median of 12 days (range 8–12) after infusion, with full resolution after a median of 3 days (range 2–6) of dexamethasone treatment **(Table 2)**.

Table 2. Incidence, severity grade, and duration of adverse events stratified by dose level.

Adverse event	Overall cohort (n = 12)	DL-3 (n = 3)	DL-2 (n = 3)	DL-1 (n = 6)
Cytokine release syndrome (CRS)				
Any-grade CRS	4 (33.3)	3	1	0
Grade 1–2 CRS	3 (25.0)	2	1	0
Grade ≥ 3 CRS	1 (8.3)	1	0	0
Median time to CRS onset, days (range)	6.5 (2–11)	2	11	–
Median time from CRS onset to resolution, days (range)	1 (1–1)	1	1	–
Immune effector cell-associated neurotoxicity syndrome (ICANS)				
Any-grade ICANS	3 (25.0)	1	1	1
Grade 1–2 ICANS	2 (16.7)	1	1	0
Grade ≥ 3 ICANS	1 (8.3)	0	0	1
Median time to ICANS onset, days (range)	12 (8–12)	8	12	12
Median time from ICANS onset to resolution, days (range)	3 (2–6)	3	2	6
Other grade ≥ 3 adverse events				
Patients experiencing grade ≥ 3 adverse events	7 (58.3)	2	1	4
Neutropenia	7 (58.3)	2	1	4
Anemia	4 (33.3)	1	0	3
Thrombocytopenia	2 (16.7)	1	0	1
Infection	2 (16.7)	1	0	1
Anorexia	1 (8.3)	1	0	0
Diarrhea	1 (8.3)	1	0	0
COVID-19 infection	1 (8.3)	0	1	0
Hypokalemia	1 (8.3)	1	0	0
Pneumonia	1 (8.3)	0	0	1
Sepsis	1 (8.3)	1	0	0

Anti-tumor activity of h1218-CART19 in patients with relapsed or refractory B-cell non-hodgkin lymphoma

Among the 12 infused patients, 1 (8.3%) exhibited primary non-response to AT101. The remaining patients achieved objective responses, resulting in an overall response rate (ORR) of 91.7% (95% CI, 56.2–97.0), including complete remission (CR) in 10 individuals (75%) **(Figures 6a-6d)**. One month after infusion, the ORR was 83.3% (95% CI, 51.6–97.9), with CR documented in eight patients (66.7%). At the three-month evaluation, among the 11 patients who remained alive, all eight responders had attained CR (72.7%) (95% CI, 43.6–92.1). Remarkably, the CR rate reached 100% when analysis was restricted to the six patients treated at higher dose levels (DL-2 and DL-3) **(Figure 6d)**. In the full study population, one patient (patient 8) who initially attained a partial response (PR) progressed before month 3. At the same time, the other responders (10/11) continued to respond, and one patient (patient 13) improved from PR to CR by month 3. After a median observation period of 9.3 months (range 1.5–16.5 months), progression-free survival (PFS) was 75.0%, and overall survival (OS) was 82.5%. Neither median PFS nor median OS had been reached at the time of analysis **(Figures 6e and 6f)**. One patient (patient 12) who had achieved CR later died from septic shock. For those who attained CR, both median PFS and OS remained unreached. These encouraging data supported selecting DL-3 as the recommended phase II dose.

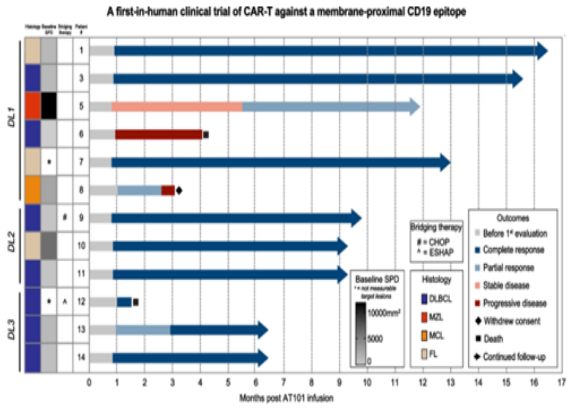

a)

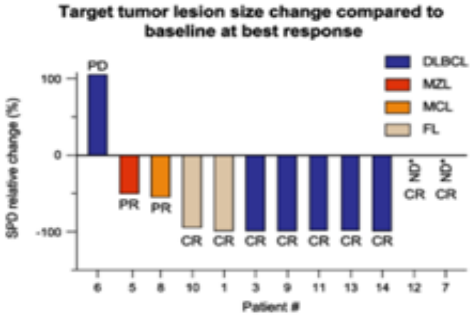

b)

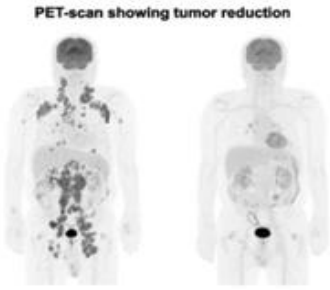

c)

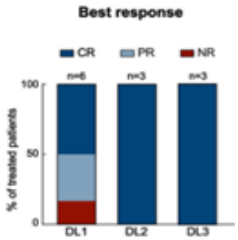

d)

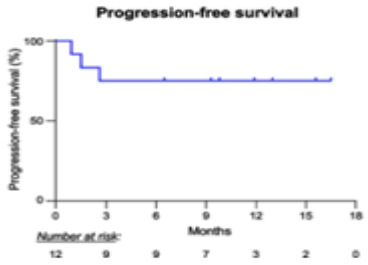

e)

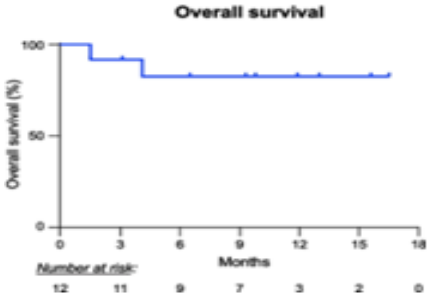

f)

Figure 6. Overview of patient features and therapeutic outcomes in the h1218-CART19 phase I study

(a) Swimmer plot displaying the clinical course and response duration for each patient following AT101 administration. Lymphoma histology and pretreatment tumor burden (sum of the product of diameters [SPD], mm^2) are annotated. See key for additional explanations. Note: patient 7 presented with non-measurable sigmoid colon involvement at infusion, while patient 12 had no measurable lesions after bridging treatment, (b) Waterfall plot summarizing the maximal percentage reduction in tumor burden from baseline for individual patients, (c) PET/CT scans of patient 10 before and one month after AT101 infusion, confirming complete metabolic response, (d) (Top) Distribution of best overall responses in the entire cohort of 12 patients. (Bottom) Best overall responses categorized by dose level (DL-1, DL-2, and DL-3), (e) Kaplan–Meier curve for progression-free survival among AT101 recipients. The number of patients at risk is indicated beneath the plot, and (f) Kaplan–Meier curve for overall survival among AT101 recipients. The number of patients at risk is indicated beneath the plot.

h1218-CART19 AT101 In Vivo Expansion, Long-Term Persistence, and Serum Cytokine Dynamics

To characterize the in vivo performance of AT101 and to explore potential associations with therapeutic efficacy and adverse reactions, CAR T-cell kinetics were monitored in peripheral blood by flow cytometry and quantitative PCR, alongside multiplex analysis of serum cytokines using the Luminex platform [29]. AT101 transgene copies in circulation reached their highest point on day 11 (range 11–14) post-infusion. A clear relationship emerged between peak expansion and the infused cell dose (DL-1: 2.5 ± 1.3, DL-2: 5.0 ± 3.4, DL-3: $113.6 \pm 6.50 \times 10^4$ CAR gene copies/µg DNA) **(Figure 7a)**. Serum cytokine monitoring demonstrated consistent post-infusion rises in several proinflammatory mediators across the patient cohort, most notably sFas ligand, granzyme A, and perforin. These molecules attained maximal concentrations around day 11 **(Figure 7b)**.

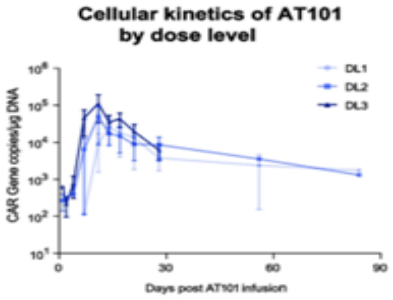

a)

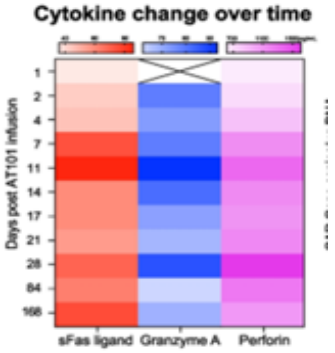

b)

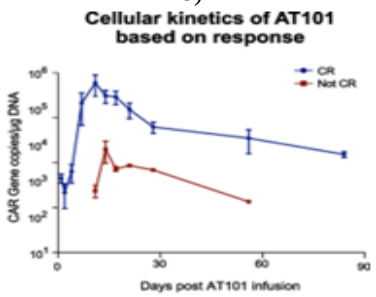

c)

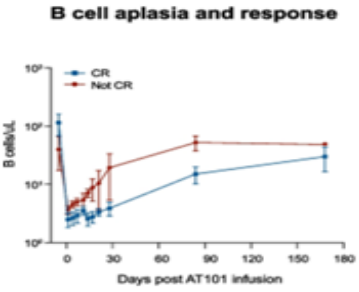

d)

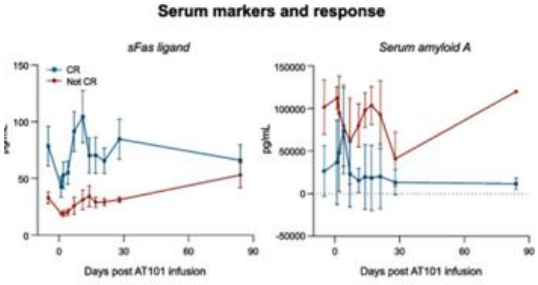

e)

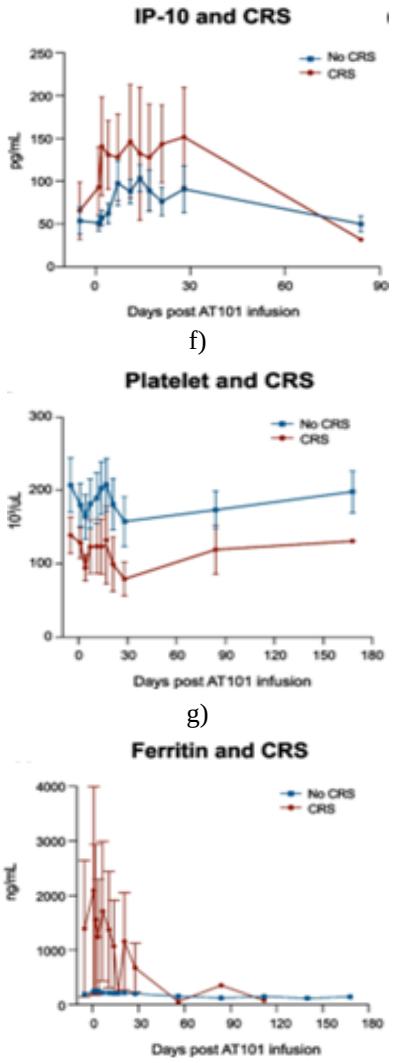

Figure 7. CAR T-cell expansion, hematologic parameters, and cytokine profiles in the h1218-CART19 phase I study

(a) Kinetics of AT101 expansion and persistence in peripheral blood quantified by qPCR for patients in DL-1, DL-2, and DL-3, (b) Average serum concentrations of sFas ligand, granzyme A, and perforin over time in all 12 patients as measured by Luminex assay, (c) Comparison of AT101 transgene expansion by qPCR between patients who attained complete response (n = 9) and those who did not (n = 3), (d) Circulating B-cell counts in patients achieving complete response (n = 9) versus non-complete response (n = 3), (e) (Left) sFas ligand and (right) serum amyloid A concentrations on day 1 (pre-infusion) and days 2–168 post-infusion in complete response versus non-complete response patients, assessed by Luminex, (f) Longitudinal changes in IP-10 serum levels in patients without cytokine-release syndrome (n = 8) compared to those with cytokine-release syndrome (n = 4), (g) Platelet count dynamics over time in patients without cytokine-release syndrome (n = 8) versus those with cytokine-release syndrome (n = 4), and (h) Ferritin concentration trajectories over time in patients without cytokine-release syndrome (n = 8) versus those with cytokine-release syndrome (n = 4).

Further evaluation revealed distinct biological patterns in patients who achieved complete remission. Peak AT101 transgene levels were markedly greater in the CR group (6.0×10^4 copies/μg DNA) than in non-CR patients (2.0×10^4 copies/μg DNA) **(Figure 7c)**. Deeper and more sustained B-cell depletion following treatment also correlated with CR status **(Figure 7d)**. sFas ligand concentrations were elevated among CR patients relative to non-CR cases. In contrast, serum amyloid A levels showed the opposite pattern, being higher in non-responders **(Figure 7e)**. Patients who developed cytokine-release syndrome exhibited amplified cytokine responses, particularly IP-10 **(Figure 7f)**, together with greater platelet reductions **(Figure 7g)**. Ferritin peaks were similarly more pronounced in the CRS subgroup compared with patients who remained free of this toxicity **(Figure 7h)**.

In summary, a novel CART19 construct was successfully advanced from preclinical development through clinical evaluation. These findings demonstrate that engagement of a membrane-proximal CD19 epitope via a CAR with rapid binding and dissociation kinetics produces robust anti-tumor activity in patients with manageable toxicity.

Therapies based on CART19 have produced impressive clinical outcomes in patients with B-cell malignancies [13, 30, 31]. Nevertheless, a substantial proportion of individuals either fail to respond initially or experience disease recurrence after treatment with existing CART19 products [32]. The primary objective of the current work was to generate and clinically evaluate a next-generation CART19 construct targeting a non-FMC63 epitope on CD19 with rapid binding and dissociation kinetics, thereby achieving superior efficacy and circumventing shared mechanisms of resistance.

Employing a chicken-derived antibody library screened against the human CD19 extracellular domain, we identified a novel anti-CD19 single-chain variable fragment (h1218) that binds a membrane-proximal

epitope with relatively low avidity. The resulting clinical product, AT101, demonstrated a favorable safety profile together with a 100% response rate at the recommended phase II dose.

All currently FDA-approved CART19 therapies rely on the same scFv derived from the FMC63 monoclonal antibody and target an identical epitope on CD19. However, malignant cells can acquire various mechanisms of resistance that promote antigen escape and subsequent relapse [8, 12, 14, 33, 34]. In particular, reduced or absent surface expression of CD19 can compromise CAR T-cell effector functions both in vitro and in vivo, while also limiting long-term CAR T-cell persistence [35]. Earlier investigations have implicated mutations within CD19 exons 2–5 as the predominant cause of antigen loss [14]. The present study specifically addressed resistance arising from loss of the FMC63 epitope, whether through point mutations in CD19 or epitope masking resulting from cis interactions between CAR19 and CD19. Our data established that h1218-CART19 exerts markedly enhanced anti-tumor effects compared with standard FMC63-based CART19 cells in preclinical models of leukemia and lymphoma. Importantly, h1218-CART19—but not FMC63-CART19—was capable of recognizing and eliminating cell lines engineered to model FMC63-resistant relapse scenarios encountered in clinical practice.

T-cell dysfunction within the immunosuppressive tumor microenvironment further constrains the capacity of CAR T cells to persist and eradicate malignant cells [36]. We postulated that refining the binding characteristics between the CAR and its target antigen could enhance CAR T-cell survival and longevity in vivo, thereby strengthening overall anti-tumor potency. Prior research has indicated that CARs with lower affinity may limit overstimulation under conditions of low antigen density, thereby reducing excessive activation and exhaustion and promoting more sustained therapeutic responses [11, 37, 38]. This benefit has been attributed largely to accelerated off-rates. In the case of h1218, we hypothesized that such kinetics would facilitate serial killing by CAR T cells—an essential feature for durable tumor control [19]. Thus, beyond targeting a distinct non-FMC63 epitope, a CAR with comparable overall affinity to FMC63-CAR but faster on- and off-rates was expected to yield superior anti-tumor performance. This design was anticipated not only to augment serial killing capacity but also to attenuate activation-induced cell death (AICD) following target engagement, ultimately improving CAR T-cell functionality.

CAR T cells are particularly vulnerable to Fas- and DR5-mediated fratricidal AICD once activation thresholds are exceeded, thereby diminishing their therapeutic potential [39]. Although genetic modifications, such as the incorporation of a dominant-negative Fas receptor, have been shown to disrupt Fas-FasL signaling and enhance CAR T-cell activity and persistence [40], such strategies often provoke heightened inflammatory cytokine release and increase the risk of severe systemic toxicities [41]. In contrast, h1218-CART19 cells exhibited milder early activation upon CD19 stimulation, coupled with superior in vivo expansion and leukemia control in xenograft models compared with FMC63-CART19. These observations are consistent with transcriptomic and phenotypic evidence that faster-off-rate CAR T cells undergo more restrained initial activation [11]. Critically, no substantial elevation in cytokine production or evidence of systemic toxicity was detected in these models. This supports earlier reports that low-avidity CAR T cells can achieve enhanced anti-tumor efficacy [11], while introducing the novel insight that improved performance can be attained even with comparable affinities by specifically accelerating off-rates. Consequently, h1218-CART19 not only offers the ability to target tumors that have lost the FMC63 epitope but also confers greater anti-tumor potency than conventional FMC63-based CART19 through the mechanism of reduced AICD.

Based on these preclinical observations, a first-in-human multicenter phase I clinical trial was initiated to assess the safety and feasibility of AT101 in individuals with relapsed or refractory non-Hodgkin lymphoma. During the phase I segment, 12 patients received escalating doses of AT101 after lymphodepletion. Among those receiving active doses (DL-2 and DL-3), both the overall response rate (ORR) and complete response rate (CRR) reached 100%. Treatment-related toxicities remained manageable, with only one instance of severe cytokine-release syndrome among the six patients treated at the higher dose levels and no cases of severe immune effector cell-associated neurotoxicity syndrome at these doses. The onset of ICANS appeared modestly delayed relative to currently approved CART19 products, potentially due to AT101's unique functional properties, although the small sample size precludes definitive conclusions. Notably, AT101 demonstrated activity across several NHL subtypes, particularly in diffuse

large B-cell lymphoma and follicular lymphoma. When restricted to these prevalent histologies, the responses observed with AT101 compare favorably to published outcomes for the FDA-approved products axicabtagene ciloleucel, lisocabtagene maraleucel, and tisagenlecleucel [32, 42], despite the modest patient numbers inherent to this early-phase study. Encouragingly, robust expansion and prolonged persistence of AT101 were documented, corroborating preclinical evidence that the lower avidity of this CAR helps shield T cells from activation-induced cell death, thereby supporting sustained proliferation beyond 30 days and extended in vivo durability. Across all patients, infusion was followed by increases in several key inflammatory cytokines, especially sFas ligand, granzyme A, and perforin. However, no substantial rises in IL-6, IL-1, GM-CSF, TNF, or IFNγ were detected, even among those experiencing toxicity. These observations imply that the combination of low avidity, rapid on- and off-rates, and recognition of an alternative epitope may produce a distinct pattern of CAR T-cell activation and a modified cytokine signature.

The treated population was heavily pretreated, with prior exposure to anti-CD19 antibodies, bispecific agents, and investigational NK-cell therapy. Despite this challenging background, no patient who attained complete remission has relapsed to date, although follow-up remains relatively brief. While preclinical experiments suggest that AT101 may circumvent certain FMC63-related resistance mechanisms, including loss of the CD19 epitope, this capability requires confirmation in larger prospective trials. It is noteworthy that no CD19-negative relapses have been observed thus far with AT101. Limitations of the study include the small cohort size and patient heterogeneity, which are typical of first-in-human early-phase trials.

Additionally, the median vein-to-vein time was longer than that of some approved CART19 therapies. Although manufacturing lead times of 1 to 2 months are common in commercial settings, it is anticipated that optimizing release testing in phase II studies will substantially shorten this interval. With the recommended phase II dose now established, the subsequent portion of the trial will evaluate AT101 efficacy specifically in relapsed or refractory diffuse large B-cell lymphoma.

Conclusion

In summary, we engineered a novel CAR-binding domain that rapidly engages an alternative membrane-proximal epitope on CD19, with rapid association and dissociation kinetics. These attributes translated into superior preclinical efficacy compared with FMC63-based CART19, driven by recognition of a distinct epitope, decreased activation-induced cell death, and more controlled activation dynamics. Translation of this approach into a first-in-human clinical trial yielded impressive clinical activity, evidenced by a 100% complete response rate at DL-2 and DL-3, accompanied by an acceptable toxicity profile.

Acknowledgments: None

Conflict of Interest: None

Financial Support: None

Ethics Statement: None

References

1. Schuster SJ, Tam CS, Borchmann P, Worel N, McGuirk JP, Holte H, et al. Long-term clinical outcomes of tisagenlecleucel in patients with relapsed or refractory aggressive B-cell lymphomas (JULIET): a multicentre, open-label, single-arm, phase 2 study. Lancet Oncol. 2021;22:1403–15.
2. Lu J, Jiang G. The journey of CAR-T therapy in hematological malignancies. Mol Cancer. 2022;21:194.
3. Vairy S, Garcia JL, Teira P, Bittencourt H. CTL019 (tisagenlecleucel): CAR-T therapy for relapsed and refractory B-cell acute lymphoblastic leukemia. Drug Des Devel Ther. 2018;12:3885–98.
4. Roberts ZJ, Better M, Bot A, Roberts MR, Ribas A. Axicabtagene ciloleucel, a first-in-class CAR T cell therapy for aggressive NHL. Leuk Lymphoma. 2018;59:1785–96.
5. Mao R, Kong W, He Y. The affinity of antigen-binding domain on the antitumor efficacy of CAR T cells: moderate is better. Front Immunol. 2022;13:1032403.
6. Ruella M, Maus MV. Catch me if you can: leukemia escape after CD19-directed T cell immunotherapies. Comput Struct Biotechnol J. 2016;14:357–62.
7. Qin H, Dong Z, Wang X, Cheng WA, Wen F, Xue W, et al. CAR T cells targeting BAFF-R can

overcome CD19 antigen loss in B cell malignancies. Sci Transl Med. 2019;11:eaaw9414.
8. Sotillo E, Barrett DM, Black KL, Bagashev A, Oldridge D, Wu G, et al. Convergence of acquired mutations and alternative splicing of CD19 enables resistance to CART-19 immunotherapy. Cancer Discov. 2015;5:1282–95.
9. Duan Y, Chen R, Huang Y, Meng X, Chen J, Liao C, et al. Tuning the ignition of CAR: optimizing the affinity of scFv to improve CAR-T therapy. Cell Mol Life Sci. 2021;79:14.
10. Ghorashian S, Kramer AM, Onuoha S, Wright G, Bartram J, Richardson R, et al. Enhanced CAR T cell expansion and prolonged persistence in pediatric patients with ALL treated with a low-affinity CD19 CAR. Nat Med. 2019;25:1408–14.
11. Michelozzi IM, Gomez-Castaneda E, Pohle RVC, Cardoso Rodriguez F, Sufi J, Puigdevall Costa P, et al. Activation priming and cytokine polyfunctionality modulate the enhanced functionality of low-affinity CD19 CAR T cells. Blood Adv. 2023;7:1725–38.
12. Ruella M, Xu J, Barrett DM, Fraietta JA, Reich TJ, Ambrose DE, et al. Induction of resistance to chimeric antigen receptor T cell therapy by transduction of a single leukemic B cell. Nat Med. 2018;24:1499–503.
13. Ruella M, Gill S. How to train your T cell: genetically engineered chimeric antigen receptor T cells versus bispecific T-cell engagers to target CD19 in B acute lymphoblastic leukemia. Expert Opin Biol Ther. 2015;15:761–6.
14. Zhang Z, Chen X, Tian Y, Li F, Zhao X, Liu J, et al. Point mutation in CD19 facilitates immune escape of B cell lymphoma from CAR-T cell therapy. J Immunother Cancer. 2020;8:e001150.
15. Kouro T, Himuro H, Sasada T. Exhaustion of CAR T cells: potential causes and solutions. J Transl Med. 2022;20:239.
16. Haso W, Lee DW, Shah NN, Stetler-Stevenson M, Yuan CM, Pastan IH, et al. Anti-CD22-chimeric antigen receptors targeting B-cell precursor acute lymphoblastic leukemia. Blood. 2013;121:1165–74.
17. James SE, Greenberg PD, Jensen MC, Lin Y, Wang J, Till BG, et al. Antigen sensitivity of CD22-specific chimeric TCR is modulated by target epitope distance from the cell membrane. J Immunol. 2008;180:7028–38.
18. Singh N, Frey NV, Engels B, Barrett DM, Shestova O, Ravikumar P, et al. Antigen-independent activation enhances the efficacy of 4–1BB-costimulated CD22 CAR T cells. Nat Med. 2021;27:842–50.
19. Roddie C, Dias J, O'Reilly MA, Abbasian M, Cadinanos-Garai A, Vispute K, et al. Durable responses and low toxicity after fast off-rate CD19 chimeric antigen receptor-T therapy in adults with relapsed or refractory B-cell acute lymphoblastic leukemia. J Clin Oncol. 2021;39:3352–63.
20. Milone MC, Fish JD, Carpenito C, Carroll RG, Binder GK, Teachey D, et al. Chimeric receptors containing CD137 signal transduction domains mediate enhanced survival of T cells and increased antileukemic efficacy in vivo. Mol Ther. 2009;17:1453–64.
21. Lee YG, Guruprasad P, Ghilardi G, Pajarillo R, Sauter CT, Patel R, et al. Modulation of BCL-2 in both T Cells and Tumor Cells to Enhance Chimeric Antigen Receptor T cell Immunotherapy against Cancer. Cancer Discov. 2022;12:2372.
22. Liu D, Bryceson YT, Meckel T, Vasiliver-Shamis G, Dustin ML, Long EO. Integrin-dependent organization and bidirectional vesicular traffic at cytotoxic immune synapses. Immunity. 2009;31:99–109.
23. Liu D, Peterson ME, Long EO. The adaptor protein Crk controls activation and inhibition of natural killer cells. Immunity. 2012;36:600–11.
24. Schuster SJ, Svoboda J, Chong EA, Nasta SD, Mato AR, Anak O, et al. Chimeric Antigen Receptor T Cells in Refractory B-Cell Lymphomas. N Engl J Med. 2017;377:2545.
25. Lee DW, Santomasso BD, Locke FL, Ghobadi A, Turtle CJ, Brudno JN, et al. ASTCT consensus grading for cytokine release syndrome and neurologic toxicity associated with immune effector cells. Biol Blood Marrow Transplant. 2019;25:625–38.
26. Cheson BD, Fisher RI, Barrington SF, Cavalli F, Schwartz LH, Zucca E, et al. Recommendations for initial evaluation, staging, and response assessment of Hodgkin and non-Hodgkin lymphoma: the Lugano classification. J Clin Oncol. 2014;32:3059–68.
27. Sommermeyer D, Hill T, Shamah SM, Salter AI, Chen Y, Mohler KM, et al. Fully human CD19-

specific chimeric antigen receptors for T-cell therapy. Leukemia. 2017;31:2191–9.
28. Xiong W, Chen Y, Kang X, Chen Z, Zheng P, Hsu YH, et al. Immunological synapse predicts effectiveness of chimeric antigen receptor cells. Mol Ther. 2018;26:963–75.
29. Kalos M, Levine BL, Porter DL, Katz S, Grupp SA, Bagg A, et al. T cells with chimeric antigen receptors have potent antitumor effects and can establish memory in patients with advanced leukemia. Sci Transl Med. 2011;3:95ra73.
30. Kochenderfer JN, Dudley ME, Kassim SH, Somerville RP, Carpenter RO, Stetler-Stevenson M, et al. Chemotherapy-refractory diffuse large B-cell lymphoma and indolent B-cell malignancies can be effectively treated with autologous T cells expressing an anti-CD19 chimeric antigen receptor. J Clin Oncol. 2015;33:540–9.
31. Ying Z, Huang XF, Xiang X, Liu Y, Kang X, Song Y, et al. A safe and potent anti-CD19 CAR T cell therapy. Nat Med. 2019;25:947–53.
32. Ghilardi G, Braendstrup P, Chong EA, Schuster SJ, Svoboda J, Ruella M. CAR-T TREK through the lymphoma universe, to boldly go where no other therapy has gone before. Br J Haematol. 2021;193:449–65.
33. Chu SH, Small D. Mechanisms of resistance to FLT3 inhibitors. Drug Resist Updat. 2009;12:8–16.
34. Mullighan CG, Phillips LA, Su X, Ma J, Miller CB, Shurtleff SA, et al. Genomic analysis of the clonal origins of relapsed acute lymphoblastic leukemia. Science. 2008;322:1377–80.
35. Ramakrishna S, Highfill SL, Walsh Z, Nguyen SM, Lei H, Shern JF, et al. Modulation of target antigen density improves CAR T-cell functionality and persistence. Clin Cancer Res. 2019;25:5329–41.
36. Cerrano M, Ruella M, Perales MA, Vitale C, Faraci DG, Giaccone L, et al. The advent of CAR T-cell therapy for lymphoproliferative neoplasms: integrating research into clinical practice. Front Immunol. 2020;11:888.
37. Caraballo Galva LD, Jiang X, Hussein MS, Zhang H, Mao R, Brody P, et al. Novel low-avidity glypican-3 specific CARTs resist exhaustion and mediate durable antitumor effects against HCC. Hepatology. 2022;76:330–44.
38. Hoseini SS, Dobrenkov K, Pankov D, Xu XL, Cheung NK. Bispecific antibody does not induce T-cell death mediated by chimeric antigen receptor against disialoganglioside GD2. Oncoimmunology. 2017;6:e1320625.
39. Kunkele A, Johnson AJ, Rolczynski LS, Chang CA, Hoglund V, Kelly-Spratt KS, et al. Functional tuning of CARs reveals signaling threshold above which CD8+ CTL antitumor potency is attenuated due to cell Fas-FasL-dependent AICD. Cancer Immunol Res. 2015;3:368–79.
40. Yamamoto TN, Lee PH, Vodnala SK, Gurusamy D, Kishton RJ, Yu Z, et al. T cells genetically engineered to overcome death signaling enhance adoptive cancer immunotherapy. J Clin Invest. 2019;129:1551–65.
41. Cox MJ, Manriquez Roman C, Tapper EE, Siegler EL, Chappell D, Durrant C, et al. GM-CSF disruption in CART cells modulates T cell activation and enhances CART cell anti-tumor activity. Leukemia. 2022;36:1635–45.
42. Sureda A, Lugtenburg PJ, Kersten MJ, Subklewe M, Spanjaart A, Shah NN, et al. Cellular therapy in lymphoma. Hematol Oncol. 2023; doi:10.1002/hon.3200